Zoosyst. Evol. 96 (2) 2020, 431–447 | DOI 10.3897/zse.96.52484

PENSOFT

MUSEUM FÜR NATURKUNDE BERLIN

A new species of *Dugesia* (Platyhelminthes, Tricladida, Dugesiidae) from China, with an account on the histochemical structure of its major nervous system

Xiao-Yu Song[1], Wei-Xuan Li[1], Ronald Sluys[2], Shu-Xin Huang[1], Shuang-Fei Li[1], An-Tai Wang[1]

1 *Shenzhen Key Laboratory of Marine Bioresource and Eco-environmental Science, Guangdong Engineering Research Center for Marine Algal Biotechnology, College of Life Sciences and Oceanography, Shenzhen University, Shenzhen, Guangdong, China*

2 *Naturalis Biodiversity Center, P.O. Box 9517, 2300 RA Leiden, The Netherlands*

http://zoobank.org/E6569135-C4D3-401F-947C-56D753ACEF67

Corresponding author: Shuang-Fei Li (sfli@szu.edu.cn)

Academic editor: A. Schmidt-Rhaesa ♦ **Received** 25 March 2020 ♦ **Accepted** 14 May 2020 ♦ **Published** 26 June 2020

Abstract

By means of an integrated approach, including molecular, morphological, anatomical and histological data, we describe a new species of freshwater flatworm of the genus *Dugesia* from southwest China, representing the third species recorded for the country. Morphologically, the new species, *Dugesia umbonata* Song & Wang, **sp. nov.**, is particularly characterised by the presence of a muscularised hump immediately antero-dorsally to a knee-shaped bend in its bursal canal and by an ejaculatory duct that opens subterminally through the dorsal side of the penis papilla. Four molecular datasets (18S rDNA; ITS-1; 28S rDNA; COI) facilitated determination of the phylogenetic position of the new species, which belongs to a clade comprising other species from the Australasian and Oriental regions. We also analysed the structure of its major nervous system by means of the acetylcholinesterase (AChE) histochemical method and compared these results with data available for three other species of *Dugesia*.

Key Words

Molecular phylogeny, taxonomy, histochemistry, acetylcholinesterase (AChE)

Introduction

The genus *Dugesia* Girard, 1850 currently comprises about 93 valid species and exhibits a distribution that comprises a major part of the Old World and Australia (see Sluys and Riutort 2018: fig. 13B). China covers a vast territory, covering six temperature zones, thus resulting in various types of climate. Therefore, it is to be expected that variations in climate and other physico-geographical conditions have resulted in a rich biodiversity of freshwater planarians, including species of *Dugesia*. However, the *Dugesia* fauna of China is very poorly known, thus far only being represented by two species. For a long time, *Dugesia japonica* Ichikawa & Kawakatsu, 1964 was the only species recorded for this country (Chen et al. 2001). It was only recently that a second species for the genus was described from southern China, viz. *Dugesia sinensis* Chen & Wang, 2015 (Chen et al. 2015).

In the present study, we describe a third, new species of *Dugesia* from southwest China on the basis of both molecular and morphological data. In addition, we document the structure of the major nervous system of the new species on the basis of a histochemical study using acetylcholinesterase (AChE) and compare its nervous system with those documented for three other species of *Dugesia*. Information on the structure of the nervous system may be useful for future phylogenetic and taxonomic studies.

Materials and methods

Specimen collection and culturing

Specimens were collected from Fengzui River in Chongqing Municipality, China (29°05.29'N, 107°10.61'E) on 8 February 2018. Animals were washed off from the underside of pebbles in the riverbed and were sampled by using 180 µm mesh sieves, after which the worms were transported to the laboratory of Shenzhen University for further analysis and culturing. The flatworms were reared in a glass aquarium (21 cm × 15 cm; depth 18 cm) with pebbles on the bottom and every day, they were fed with fresh pork liver, which was made available for about one hour, after which the aquarium was cleaned from food residues, while the water was replaced with aerated tap water. Cultures were kept at room temperature (23–26 °C).

DNA extraction, amplification, sequencing and phylogenetic analysis

The single, asexual, fissiparous animal that was available for molecular analysis was fixed in absolute ethanol after three days of starvation; it was not subjected to any anatomical examination. Total genomic DNA was extracted by using E.Z.N.A. Mollusc DNA Isolation Kit (Omega, Norcross, GA, USA). Four gene fragments were amplified by polymerase chain reaction (PCR): 18S ribosomal gene (18S rDNA), ribosomal internal transcribed spacer-1 (ITS-1), 28S ribosomal gene (28S rDNA), cytochrome C oxidase subunit I (COI). Primers used for amplification and the polymerase chain reaction (PCR) protocol are listed in Suppl. material 1: Table S1. We used KOD One DNA Master Mix (TOYOBO, Japan) to amplify 18S rDNA, 28S rDNA and COI. For unknown reasons, we failed to amplify ITS-1 with KOD One DNA Master Mix and, therefore, this gene was amplified with 2×Taq Plus Master Mix II (Vazyme, China). The amplified sequences of each gene were all taken from a single individual. Both strands of DNA were determined by Sanger sequencing either at BGI (Shenzhen, China) or Beijing TsingKe Biotech Co. Ltd. (Beijing, China). All new sequences have been uploaded to GenBank, NCBI (Table 1).

Sequences of other taxa used in the phylogenetic analysis were downloaded from GenBank, NCBI (Table 1). In order to determine the phylogenetic position of our new Chinese specimens within the genus *Dugesia*, four datasets were generated, comprising as in-group sequences of the newly collected specimen, as well as all available sequences of *Dugesia* species (19 taxa for 18S rDNA, 34 taxa for ITS-1, 19 taxa for 28S rDNA and 35 taxa for COI; see Table 1) and two species of its sister genera as out-groups, viz. *Recurva postrema* Sluys & Solà, 2013 (ITS-1 sequence not available in GenBank, NCBI) and *Schmidtea mediterranea* Benazzi et al., 1975. We also generated an additional COI dataset (aCOI) for assessing the nucleotide substitution saturation, including all taxa of the COI dataset, excepting *Dugesia batuensis* Ball, 1970 and *D. deharvengi* Kawakatsu & Mitchell, 1989 (two sequences with only 289 bp, which will create numerous gaps in the alignment and thus reduce the sensitivity of substitution saturation tests; Xia et al. 2003; Xia and Lemey 2009).

For ribosomal DNA, sequences were independently aligned by CLUSTAL W plug-in included in MEGA v.6.0 (Tamura et al. 2013). In order to check for the absence of stop codons, mitochondrial coding gene COI sequences were translated into amino acids by ORFFINDER in NCBI, using the genetic code 9, after which they were aligned by MACSE (Ranwez et al. 2011) in https://mbb.univ-montp2.fr/MBB/subsection/softExec.php?soft=macse (accessed 13 February 2020). Regions of ambiguous alignments were excluded by GBLOCKS v.0.91b (Talavera and Castresana 2007), using the same parameters as in Li et al. (2019). After GBLOCKS processing, the four alignments were manually combined to create a concatenated dataset in the following order: 18S rDNA–ITS-1–28S rDNA–COI. Those sequences, which were shorter or not available in GenBank, were completed with missing data (Ns). We used the substitution saturation test (Xia et al. 2003; Xia and Lemey 2009) in DAMBE6 software (Xia 2017) to assess the nucleotide substitution saturation for five datasets (18S rDNA, ITS-1, 28S rDNA, COI and aCOI).

In order to find the best-fit evolutionary models, we used MRMODELTEST v 2.3 (Nylander 2004) by applying the Akaike Information Criterion (AIC); the GTR+G model was chosen for ITS-1, while the GTR+I+G model was chosen for the other three sets of data, viz. 18S rDNA, 28S rDNA and COI. We defined gene partitions in the concatenated dataset analyses, so that the estimation of the parameters for each partition was independent.

Two phylogenetic inference methods were used, viz. Maximum Likelihood (ML) and Bayesian Inference (BI). Both approaches were used to independently analyse each gene separately, as well as the concatenated dataset. Partitioned analysis was performed on the concatenated dataset, so that the evolutionary models chosen by MRMODELTEST were assigned to the corresponding individual genes.

We used RAXML-NG v0.9.0 (Kozlov et al. 2019) to infer phylogeny for ML, while applying the options --all (tree search and bootstrapping analysis) and --bs-trees 1000 (number of replicates). Bayesian analyses were performed in MRBAYES v3.2.6 (Ronquist et al. 2012) for each gene independently and for the concatenated dataset, with two simultaneous runs of one cold and three hot chains. Each run was performed for 1,000,000 generations for 18S rDNA and 28S rDNA analyses and 2,000,000 generations for the ITS-1 analysis, sampling every 1,000 generations. In the analyses of COI and the concatenated dataset, each run was performed for 5,000,000 generations, sampling every 5,000 genera-

Table 1. GenBank accession numbers of sequences for species taxa used in the phylogenetic analyses.

Species	18S rDNA	ITS-1	28S rDNA	COI
Recurva postrema	KF308691		MG457274	KF308763
Schmidtea mediterranea	U31085	AF047854	MG457267	JF837062
Dugesia aenigma	KF308698	KC007043		
D. aethiopica	KY498822	KY498785	KY498806	KY498845
D. afromontana	KY498823	KY498786	KY498807	KY498846
D. arcadia	KF308694	KC007047		KC006969
D. ariadnae		KC007049		JN376142
D. aurea		MK713027	MK712523	MK712632
D. batuensis		KF907816	KF907823	KF907819
D. benazzii		MK713037	MK712509	FJ646977, FJ646933
D. bengalensis		FJ646897		
D. bifida	KY498843	KY498791	KY498813	KY498851
D. bijuga	MH113806			MH119630
D. corbata		MK713029	MK712525	MK712637
D. cretica	KF308697	KC007055		KC006974
D. damoae		KC007057		KF308768
D. deharvengi		KF907817	KF907824	KF907820
D. effusa		KC007058		KF308780
D. elegans	KF308695	KC007063		KC006985
D. etrusca		FJ646898		MK712651
D. gibberosa	KY498842	KY498803	KY498819	KY498857
D. gonocephala	DQ666002	FJ646901	DQ665965	FJ646941, FJ646986
D. granosa	KY498833	KY498795	KY498816	
D. hepta		MK713035	MK712512	MK712639
D. ilvana		FJ646903		FJ646989, FJ646944
D. improvisa	KF308696	KC007065		KF308774
D. japonica	D83382	FJ646906	DQ665966	AB618487
D. liguriensis		FJ646907		MK712645
D. malickyi		KC007069		KF308750
D. naiadis				KF308757
D. notogaea	KJ599713	FJ646908	KJ599720	FJ646993, FJ646945
D. parasagitta		KC007073		KF308739
D. pustulata	MH113807			MH119631
D. ryukyuensis	AF050433	FJ646910	DQ665968	AB618488
D. sagitta		KC007085		KC007006
D. sicula	KF308693	FJ646915	DQ665969	KF308797
D. sigmoides	KY498827	KY498789	KY498811	KY498849
D. sinensis				KP401592
D. subtentaculata	AF013155	MK712995	MK712493	MK712561
D. umbonata	MT177214*	MT177211*	MT177210*	MT176641*
D. vilafarrei		MK712997	MK712511	MK712648

* Sequences from this study.

tions. The first 25% of the generated trees were discarded as burn-in to obtain the consensus tree and posterior probability values (pp). In order to ensure that the chains had reached the stationary region, we terminated the two runs when the average standard deviation of split frequencies was consistently lower than 0.01. We checked the *.p* file of each run in TRACER v1.7.1 (Rambaut et al. 2018) to ensure that the effective sample size (ESS) values of each parameter were above 200.

Histology

Three-day starved mature individuals were placed onto a watch glass, after which modified Bouin's fixative (saturated nitric acid: formaldehyde: glacial acetic acid = 68:25:7) was poured over a worm when it was fully extended. Hereafter specimens were transferred to a weighing bottle (40 × 25 mm) positioned on a laboratory shaker and thus were fixed for 24 hours in modified Bouin's fluid. Hereafter, they were washed in 75% ethanol, dehydrated in an ascending series of ethanol baths, cleared in terpineol and embedded in wax (Paraplast Plus, Sigma). Histological sections were made at intervals of 6 µm.

Preparations were stained with both modified Cason's Mallory-Heidenhain stain and haematoxylin (see Yang et al. 2020). Histological sections of PLA-0152–PLA-0154 and RMNH.VER.19968.a were mounted with neutral balsam (Shanghai Yuanye Biotechnology Co. Ltd.), while specimens PLA-0151 and RMNH.VER.19968.b were mounted with DPX (Head Biotechnology Co. Ltd., Beijing). The preparations PLA-151–PLA-154 were deposited in the Institute of Zoology, Chinese Academy of Sciences (IZCAS), Beijing, China, while RMNH.VER.19968.a and RMNH.VER.19968.b were deposited at Naturalis Biodiversity Center, Leiden, The Netherlands.

AChE histochemistry

For preparation of solutions and reagents used in the histochemical study, see Suppl. material 2: Table S2. We chose asexual, fissiparous specimens for the experiment because: (a) small specimens are easier to handle under the microscope, (b) it is difficult to perform the histochemical reaction in large specimens, the abundance of mucus causing major problems and (c) observation of the nervous system is more difficult in larger and therefore, usually, somewhat thicker specimens. The animals were starved for seven days before the start of the experiment. Randomly selected starved specimens were cut transversely into pieces of 2–3 mm, on average, thereby avoiding damage to the pharynx. Hereafter the fragments were left to regenerate in clean mineral water for 10 days. Regenerated worms were placed onto a glass slide and then killed by a few drops of 10% acetic acid when the specimens were fully extended and, subsequently, they were washed for 20 s in phosphate buffer. Hereafter, a few drops of 4% paraformaldehyde were added, after which a 10 mm × 10 mm coverslip was applied, after which the glass slide was put on ice and the specimen was left under the coverslip for 15 min, thus being slightly squashed. Hereafter, specimens were transferred to a weighing bottle (40 × 25 mm) with 4% paraformaldehyde and fixed at 4 °C for 24 h. Then the worms were transferred to four 10 min baths of phosphate buffer on a shaker and, subsequently, transferred to a bath of 3% Triton X-100 for 1 h on a shaker. The specimens were then transferred to three 10 min baths of the acetate buffer on a shaker. All steps mentioned above were performed in an ice bath to maintain a solution temperature of about 4 °C.

The reaction solution was made 60 min before use and consisted of the following components, which were mixed while on a shaker, in the following order: acetylcholinesterase solution 0.5 ml + 0.82% sodium acetate 3.1 ml + 0.6% acetic acid 0.1 ml + 2.94% sodium citrate 0.3 ml + 0.75% copper sulphate 0.45 ml + 0.165% potassium ferricyanide 0.65 ml. Specimens were treated with this solution for 60–120 min until the nervous system appeared copper-red. The histochemical reaction was stopped by three baths in distilled water, whereafter the specimens were transferred to a glass slide for observation under a compound microscope. The specimens were temporarily mounted in distilled water and were discarded after examination.

Abbreviations used in the figures

bc: bursal canal; ca: common atrium; cb: copulatory bursa; ceg: cement gland; cg: cerebral ganglion; coa: copulatory apparatus; d: diaphragm; e: eye; ed: ejaculatory duct; go: gonopore; h: hump; lod: left oviduct; m: mouth; ma: male atrium; ov: ovary; pg: penis glands; ph: pharynx; pp: penis papilla; rod: right oviduct; sg: shell gland; sv: seminal vesicle; tc: transverse commissure; tn: transverse nerves; vd: vas deferens; vnc: ventral nerve cord.

Results

Datasets

The amplified sequences of each gene of the new species have the following lengths: 18S rDNA: ~1700 base pairs (bp); ITS-1: ~700 bp; 28S rDNA: ~1600 bp; COI: ~900 bp. For phylogenetic analyses, five datasets were generated, viz. 18S rDNA, ITS-1, 28S rDNA, COI and a concatenated dataset.

After GBLOCKS processing, the 18S rDNA dataset contained 22 OTUs with a total length of 1221 bp, the ITS-1 dataset contained 36 OTUs and 544 bp, the 28S rDNA dataset included 22 OTUs and 1352 bp, while the COI dataset comprised 38 OTUs and 693 bp (Table 1). The concatenated dataset contained 41 OTUs and 3810 bp, divided as follows: 1221 bp for 18S rDNA, 544 bp for ITS-1, 1352 bp for 28S rDNA and 693 bp for COI.

Saturation analysis revealed that the three non-coding gene datasets (18S rDNA, ITS-1 and 28S rDNA) exhibited only low levels of substitution saturation (Iss < Iss.c with significant difference; nos. 1–6 in Suppl. material 3: Table S3), irrespective of inclusion of all sites or only fully-resolved sites. The COI dataset showed high levels of saturation in case of an asymmetrical tree (Iss > Iss.cAsym; nos. 7, 9 & 11 in Suppl. material 3: Table S3), irrespective of inclusion of codon positions 1 and 2 or codon position 3 or all three positions together. However, the COI dataset showed no or very little saturation when only the fully resolved sites were analysed (nos. 8, 10 & 12 in Suppl. material 3: Table S3). In case of the aCOI dataset, i.e. with exclusion of the two short sequences, no saturation was apparent when codon positions 1 and 2 or all three positions were included (nos. 13–16 in Suppl. material 3: Table S3). However, the third codon position was more or less saturated, except in case of a symmetrical tree analysed with only fully-resolved sites (nos. 17 and 18 in Suppl. material 3: Table S3).

Molecular phylogeny

The phylogenetic trees constructed by BI and ML methods for the four genes, as well as the concatenated dataset, are identical or basically similar in topology, differing only in those nodes that were weakly supported (Fig. 1 and Suppl. material 4: Figs S1–S6). It should be noted that not all species were included in all trees, due to the lack of molecular data for some of the genes.

In the phylogenetic tree obtained from the concatenated dataset, the new species described below, viz. *Dugesia umbonata* Song & Wang, sp. nov., clusters together with *D. japonica* with high support values (1.00 posterior probability – pp; 98% bootstrap – bs; Fig. 1 and Suppl.

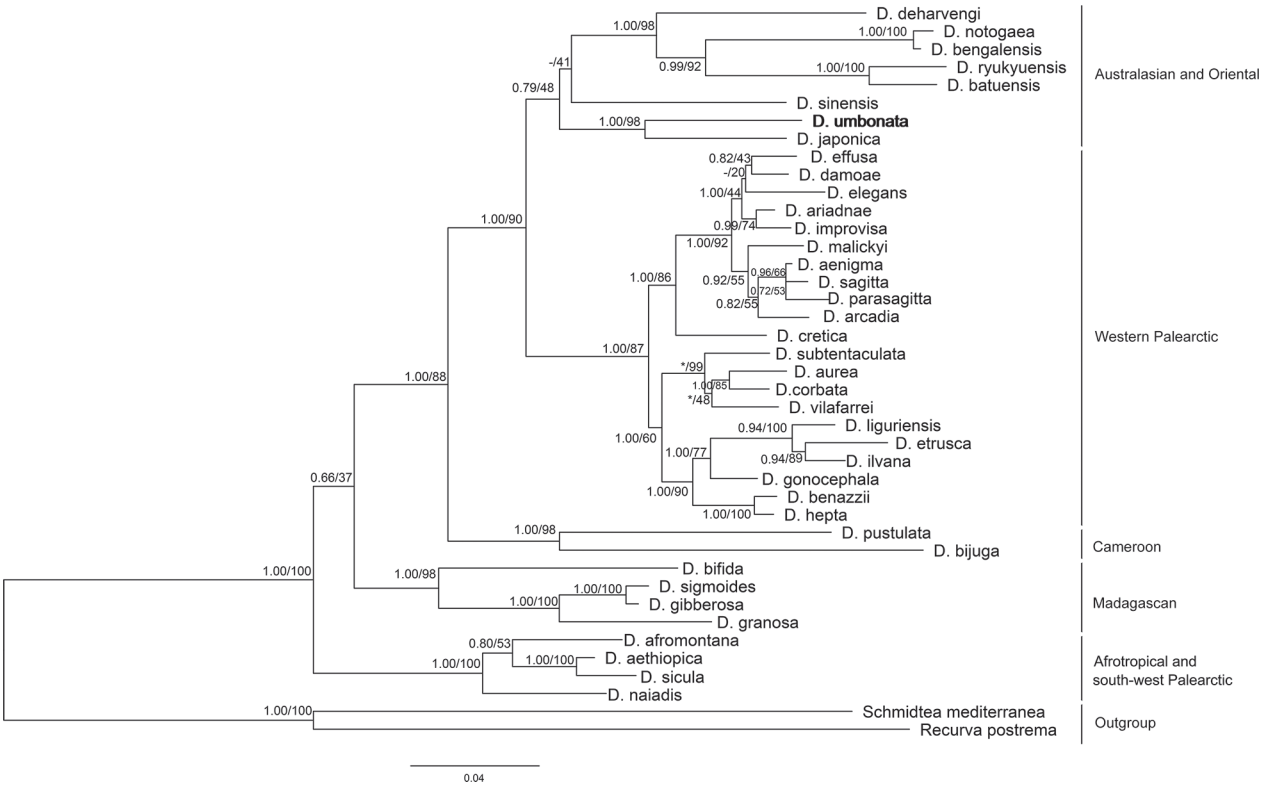

Figure 1. Maximum likelihood phylogenetic tree topology inferred from the concatenated dataset (18S rDNA, ITS-1, 28S rDNA and COI). Numbers at nodes indicate support values (posterior probability/bootstrap). *: Bootstrap value not applicable to this node, because of different topologies of trees generated by BI and ML methods.

material 4: Fig. S1). The branches leading to these two species are long, indicating a high divergence between these two species (Fig. 1 and Suppl. material 4: Fig. S1), which constitute a clade with the species *Dugesia deharvengi*, *D. notogaea*, *D. bengalensis*, *D. ryukyuensis*, *D. batuensis* and *D. sinensis*, albeit with rather low support values (0.79 pp; 48% bs; Fig. 1 and Suppl. material 4: Fig. S1). All species in this clade occur in the Australasian and Oriental biogeographic regions.

In the trees based on COI, *D. umbonata* shares the same affinities as revealed by the trees obtained from the concatenated dataset, albeit that the nodes are only weakly supported (Suppl. material 4: Figs S2, S3).

In the 18S rDNA tree, *D. umbonata* is sister to *D. japonica* and together, they share a sister-group relationship with a species group comprising nine Afrotropical and Cameroon species (*D. granosa*, *D. gibberosa*, *D. sigmoides*, *D. bifida*, *D. sicula*, *D. aethiopica*, *D. afromontana*, *D. pustulata* and *D. bijuga*), albeit with rather low support value (0.61 pp; 47% bs; Suppl. material 4: Fig. S4).

With respect to the 28S rDNA tree, it is noteworthy that *D. umbonata* and *D. japonica* occupy completely different positions, as compared with all other trees generated (Fig. 1, Suppl. material 4: Figs S1–S4, S6). They cluster together as sister species, but then share a sister-group relationship, albeit with rather low support (37% bs), with seven species from the western Palearctic region (*D. subtentaculata*, *D. vilafarrei*, *D. corbata*, *D. aurea*, *D. hepta*, *D. benazzii* and *D. gonocephala*; Suppl. material 4: Fig. S5).

In the ITS-1 tree, the situation is again different in that *D. umbonata* is sister to a species-group comprising *D. japonica*, *D. deharvengi*, *D. notogaea*, *D. bengalensis*, *D. ryukyuensis* and *D. batuensis*, albeit with low support values (0.91 pp; 55% bs; Suppl. material 4: Fig. S6).

In our trees obtained from the concatenated dataset, five biogeographic groups are supported weakly at their nodes, viz. (1) Australasian and Oriental, (2) Western Palearctic, (3) Cameroon, (4) Madagascan and (5) Afrotropical and south-west Palearctic. The Australasian and Oriental group (from *D. deharvengi* to *D. japonica* in Fig. 1), shares a sister-group relationship with the Western Palearctic group (from *D. effusa* to *D. hepta* in Fig. 1), supported by no less than 1.00 pp, but only by 90% bs, while this clade clusters together with the species-group from Cameroon (comprising *D. bijuga* and *D. pustulata*), supported by 1.00 pp, but only 88% bs. In turn, the clade formed by the Asian, Australian, European and Cameroon species is sister to the Madagascan group (comprising *D. bifida*, *D. sigmoides*, *D. gibberosa* and *D. granosa*), with rather low support values (0.66 pp; 37% bs). The Afrotropical and south-west Palearctic group (comprising *D. afromontana*, *D. aethiopica*, *D. sicula* and *D. naiadis*) is the first to branch off, with rather high support value (1.00 pp; 100% bs).

Systematic Account

Order Tricladida Lang, 1884
Suborder Continenticola Carranza, Littlewood, Clough, Ruiz-Trillo, Baguñà & Riutort, 1998
Family Dugesiidae Ball, 1974
Genus *Dugesia* Girard, 1850

***Dugesia umbonata* Song & Wang, sp. nov.**
http://zoobank.org/126FAA7D-9B17-42C8-BCFA-BF7AEF9FA9F6

Material examined. Holotype: PLA-0151, Fengzui River, Chongqing, China, 29°05.29'N, 107°10.61'E, 8 February 2018, coll. Xiao-Zhou Hu, sagittal sections on 24 slides.

Paratypes: PLA-0152, ibid., sagittal sections on 28 slides; PLA-0153, ibid, horizontal sections on 8 slides; PLA-0154, ibid., transverse sections on 27 slides; RMNH.VER.19968.a, ibid., sagittal sections on 18 slides; RMNH.VER.19968.b, ibid., sagittal sections on 27 slides.

Habitat. Specimens were collected from a shallow tributary of Fengzui River (29°05.29'N, 107°10.61'E), the latter located at the western side of Jinfo Mountain at an altitude of about 530 m above sea level (a.s.l.) (Fig. 2A). The Fengzui River is a tributary of Wujiang River, while the latter is a tributary of the Yangtse River (Fig. 2A). The animals were collected from the underside of small pebbles in the riverbed (Fig. 2B, C), which had a water depth of 3–10 cm; air temperature was about 9 °C. Only 15 specimens were collected at the beginning, none of which was sexually mature. After about 1.5 years of rearing under laboratory conditions, in total about 40 specimens eventually sexualised.

Diagnosis. A blackish species of *Dugesia* characterised by the following characters: muscularised hump immediately antero-dorsally to a knee-shaped bend in its bursal canal; ejaculatory duct opening subterminally through the dorsal side of the penis papilla; oviducts opening asymmetrically into the female copulatory apparatus, with the right oviduct opening into the knee-shaped bend of the bursal canal and the left oviduct opening into the common atrium; an asymmetrical penis papilla; small diaphragm; presence of a duct between seminal vesicle and diaphragm.

Etymology. The specific epithet is based on the Latin *umbonis*, rounded protuberance, and alludes to the muscularised hump that sits on the postero-dorsal portion of the bursal canal.

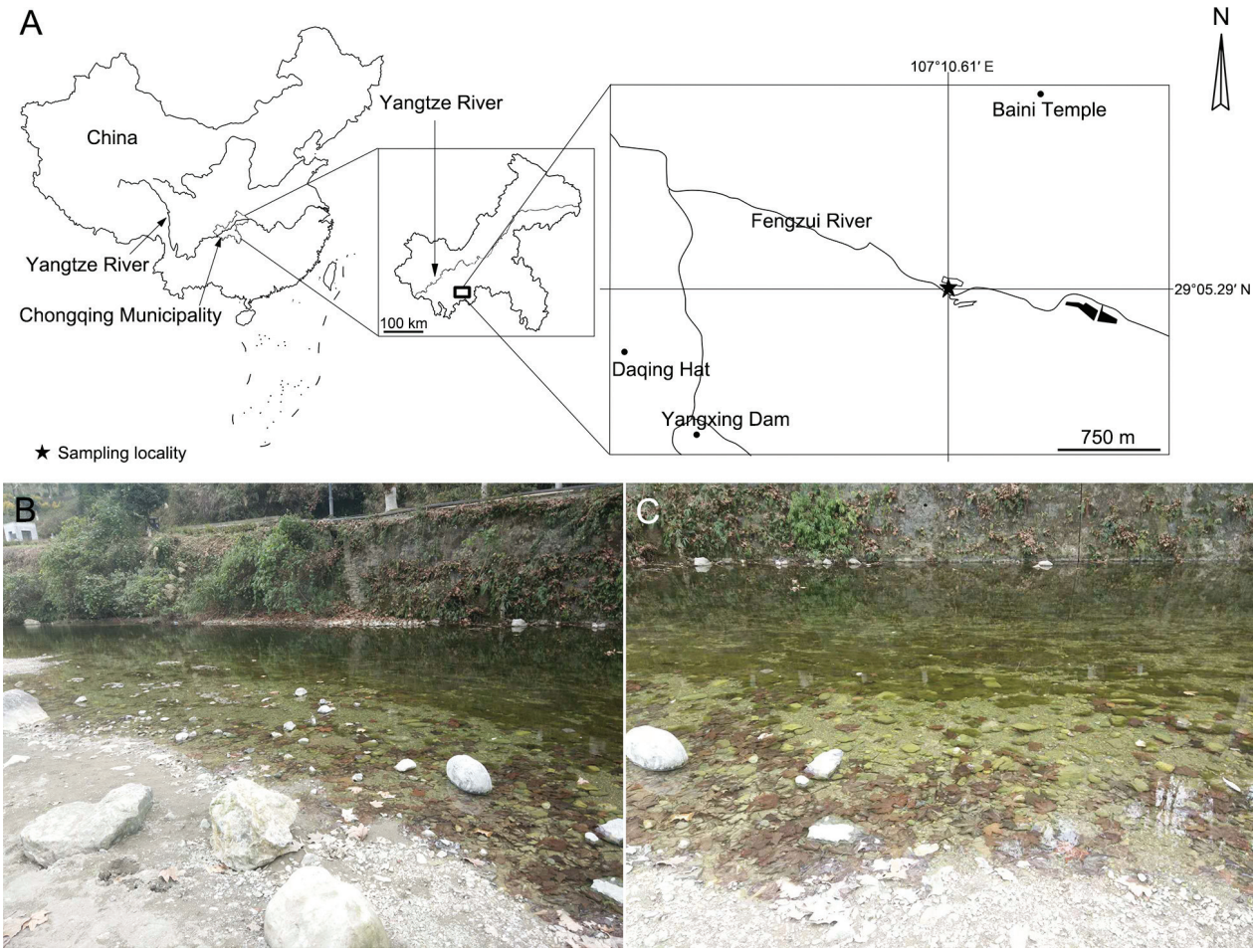

Figure 2. Locality and habitat of *Dugesia umbonata*. **A.** sampling locality in Chongqing Municipality, China; **B, C.** habitat at sampling locality.

Description. Fissiparous and ex-fissiparous animals exhibit similar external features, apart from body size. Description and measurements, presented below, are based on sexualised, ex-fissiparous specimens.

Living, sexualised ex-fissiparous specimens ranged from 1.93–3.14 cm in length and 1.97–3.44 mm in width (n = 5; Fig. 3A, B). A pair of eyes is located at about 1/21 of the body length as determined from the anterior body end (Figs 3A, B, 4A). The distance between the eyes and the lateral body margin varies from 369–478 µm (n = 5), while the distance between the eye cups ranges from 129–297 µm (n = 5; Figs 3A, B, 4A). Each eye cup contains numerous retinal cells. Auricular grooves are located near the body margins on either side of the head, at a position just posterior to the eyes (Figs 3A, B, 4A).

The dorsal surface is blackish, the colouration being formed by dense accumulations of dark brown specks; the ventral surface is brown (Figs 3, 4). Regions around the eyes and auricular grooves are unpigmented (Figs 3A, B, 4A). A pale, narrow mid-dorsal stripe runs from anterior to the eyes to the tip of the tail; body margins are also pale (Figs 3A, B, 4A).

The cylindrical pharynx is positioned at about 2/5–1/2 of the body length as determined from the anterior body margin (Fig. 3); it measures about 1/10 of the total body length, i.e. about 2.26–3.01 mm in length and 129–297 µm in width (n = 5; Figs 3A, B, 4C). The outer epithelium of the pharynx is underlain by a thick layer of longitudinal muscle, followed by 2–3 layers of circular muscle. The inner epithelium is underlain by a rather thick layer of circular muscles, followed by 2–3 layers of longitudinal muscle. The mouth opening is situated at the posterior end of the pharyngeal cavity (Fig. 4C).

A pair of hyperplasic ovaries is situated at a short distance behind the brain, i.e. at about 1/10–3/20 of the body length as determined from the anterior body margin (n = 5; Figs 3A, B, 4B), the gonads measuring about 471–1049 µm in anterior-posterior direction and about 149–234 µm in width (n = 5; Figs 3A, 4B).

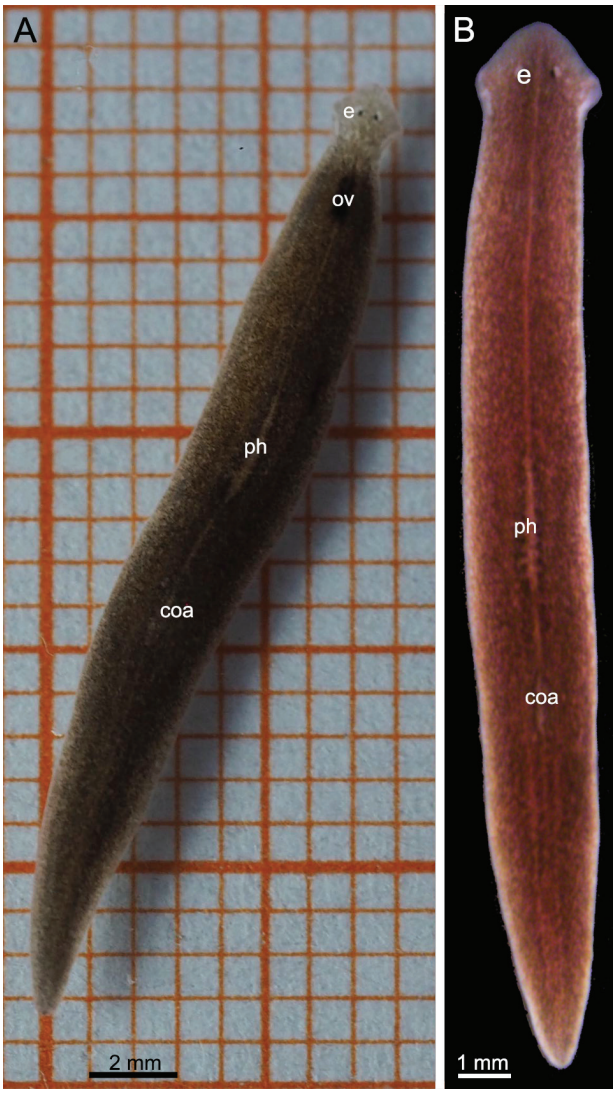

Figure 3. *Dugesia umbonata*. **A, B.** habitus of live, sexual animals in dorsal view.

The oviducts open asymmetrically into the female copulatory apparatus, with the right oviduct opening into the knee-shaped bend of the bursal canal,

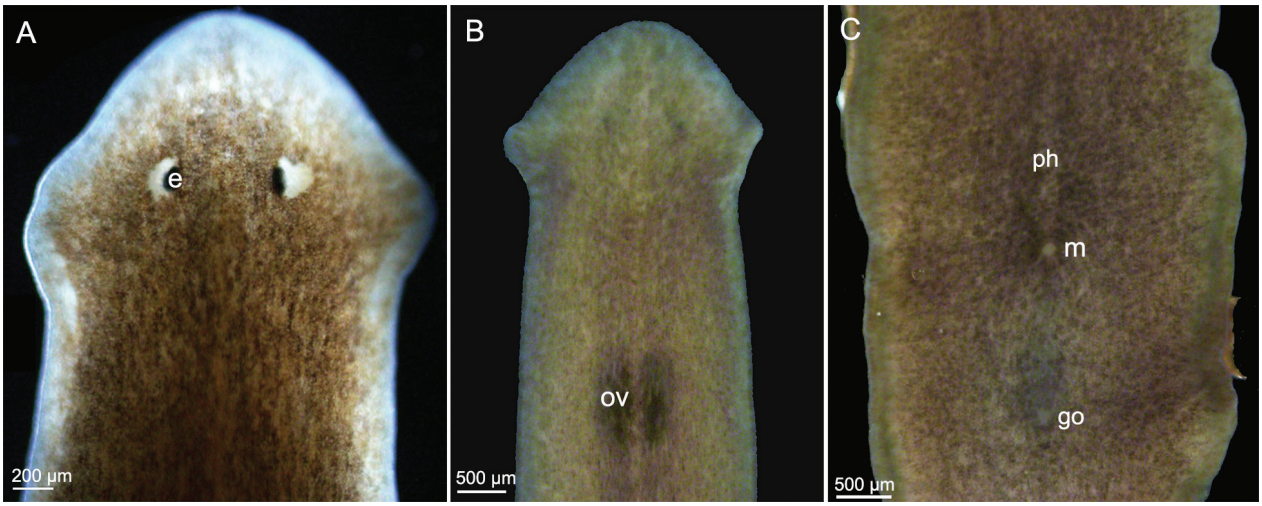

Figure 4. *Dugesia umbonata*, habitus of live animals. **A.** anterior end, dorsal view; **B.** ventral view of anterior end showing ovaries; **C.** ventral view of rear end, showing pharynx, mouth and gonopore.

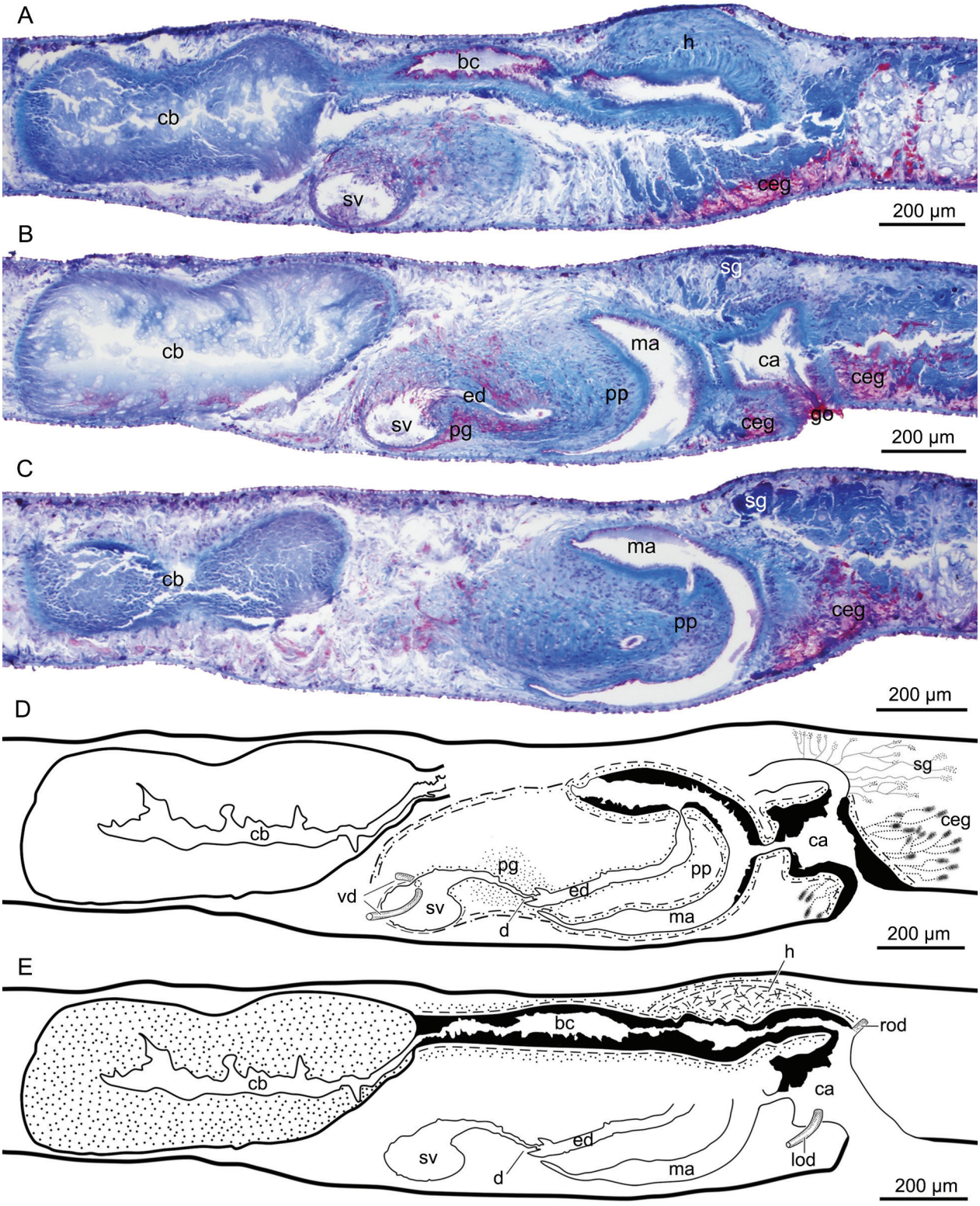

Figure 5. *Dugesia umbonata*, holotype PLA-0151, sagittal sections and reconstructions of the copulatory apparatus. **A.** photomicrograph showing copulatory bursa, bursal canal, hump and seminal vesicle; **B.** photomicrograph showing copulatory bursa, seminal vesicle, ejaculatory duct, diaphragm, penis, male atrium, common atrium and gonopore; **C.** photomicrograph showing copulatory bursa, ejaculatory duct, penis papilla and male atrium; **D.** reconstruction male copulatory apparatus; **E.** reconstruction female copulatory apparatus.

while the left oviduct opens into the common atrium (Figs 5E, 6E, 7E).

A large, elongated, sac-shaped copulatory bursa is situated posteriorly to the pharynx and is lined with a layer of vacuolated, nucleated cells (Figs 5–7). The bursal canal runs from the postero-dorsal wall of the copulatory bursa in a caudal direction to the left-side of the copulatory apparatus. Hereafter, the bursal canal makes a knee-shaped

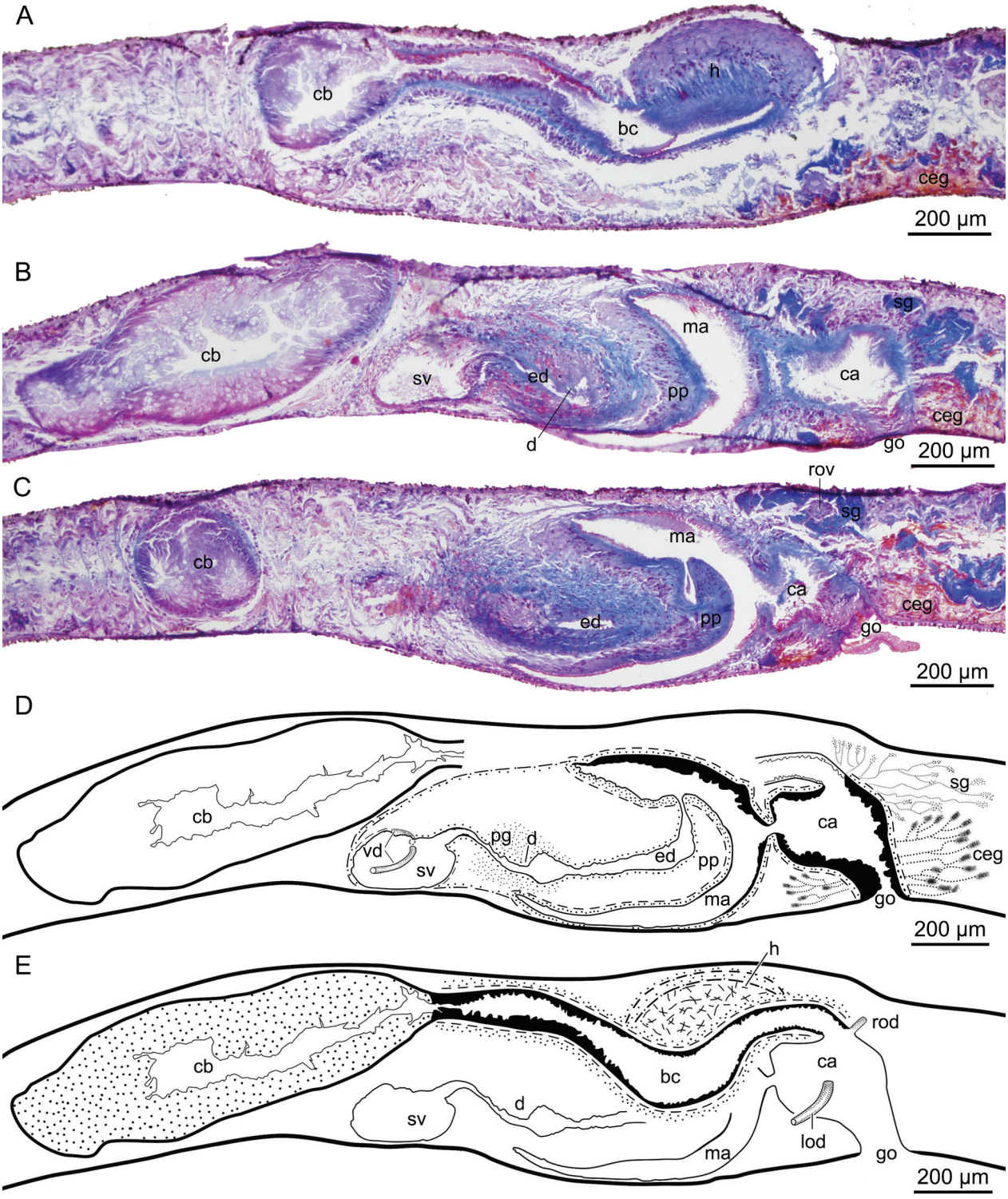

Figure 6. *Dugesia umbonata*, paratype PLA-0152, sagittal sections and reconstructions of the copulatory apparatus. **A.** photomicrograph showing copulatory bursa, bursal canal and hump; **B.** photomicrograph showing copulatory bursa, seminal vesicle, ejaculatory duct, diaphragm, penis, male atrium, common atrium and gonopore; **C.** photomicrograph showing copulatory bursa, ejaculatory duct, penis, male atrium and common atrium; **D.** reconstruction male copulatory apparatus; **E.** reconstruction female copulatory apparatus.

bend in the antero-ventral direction, after which it opens into the dorsal portion of the common atrium (Figs 5A, B, E, 6A, E, 7A, E). The bursal canal is lined by a nucleated, glandular epithelium, which is underlain by 2–3 layers of longitudinal muscles, followed by 6–8 layers of circular muscle. Shell glands discharge their cyanophilic secretion into the knee-shaped portion of the bursal canal (Figs 5B–D, 6B–D, 7B–D).

Immediately antero-dorsally to the knee-shaped bend, the bursal canal carries a voluminous, ellipsoidal

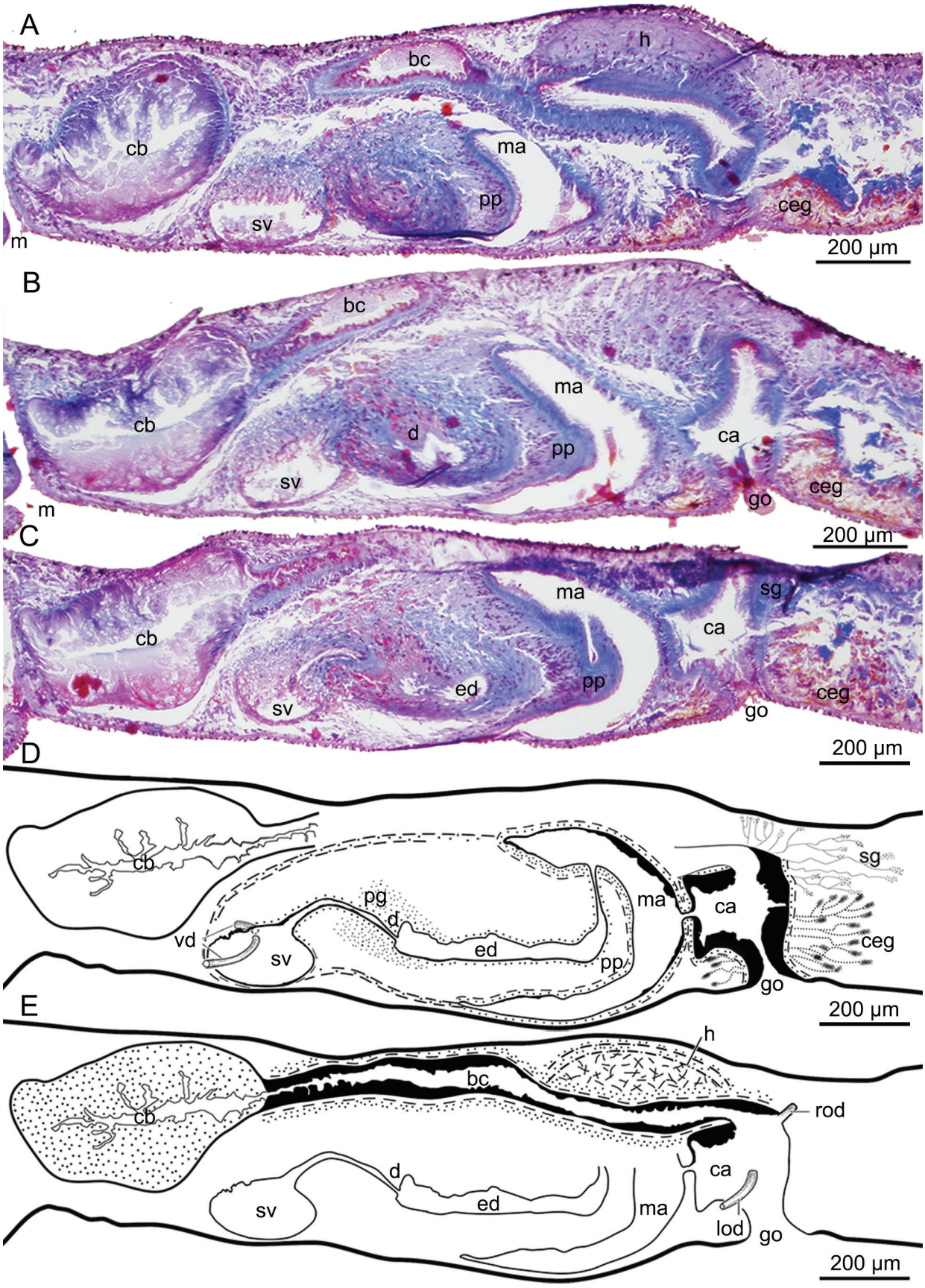

Figure 7. *Dugesia umbonata*, paratype RMNH.VER.19968.a, sagittal sections and reconstructions of the copulatory apparatus. **A.** photomicrographs showing copulatory bursa, bursal canal, seminal vesicle, diaphragm, penis, male atrium and hump; **B.** photomicrograph showing copulatory bursa, bursal canal, seminal vesicle, diaphragm, penis, male atrium, common atrium and gonopore; **C.** photomicrograph showing copulatory bursa, ejaculatory duct, penis, male atrium, common atrium and gonopore; **D.** reconstruction male copulatory apparatus; **E.** reconstruction female copulatory apparatus.

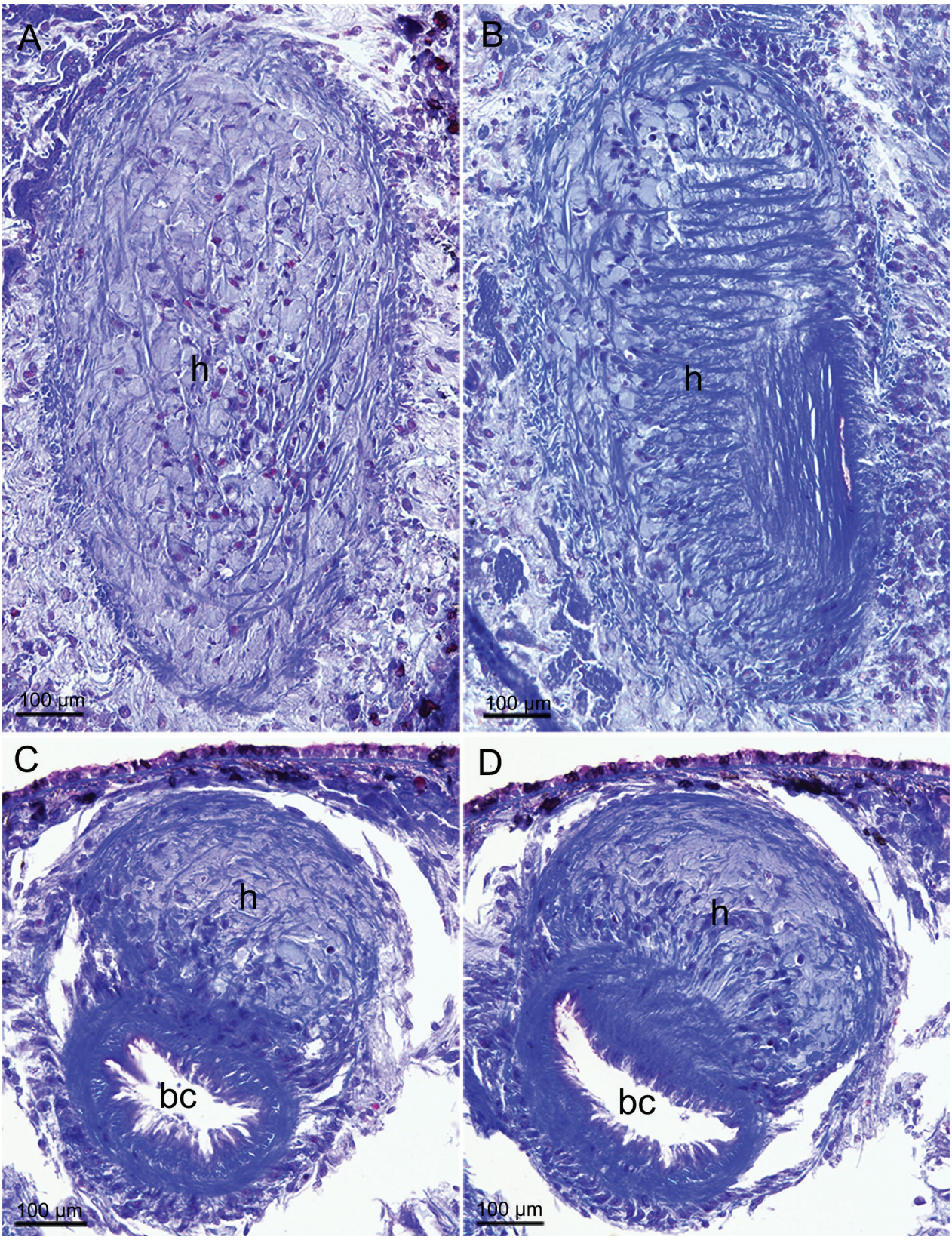

Figure 8. *Dugesia umbonata*, photomicrographs showing the hump. **A, B.** paratype PLA-0153, horizontal sections (anterior at the top); **C, D.** paratype PLA-0154, transverse sections.

muscular hump that measures about 428–475 µm in anterior-posterior direction and 268–292 µm in cross-section (n = 3; Figs 5A, E, 6A, E, 7A, E). The hump consists of irregular, nucleated mesenchymal cells and is surrounded by a coat of intermingled muscles; there are also muscle fibres traversing the hump in all directions in a more loosely arranged, irregular and reticulated way (Fig. 8).

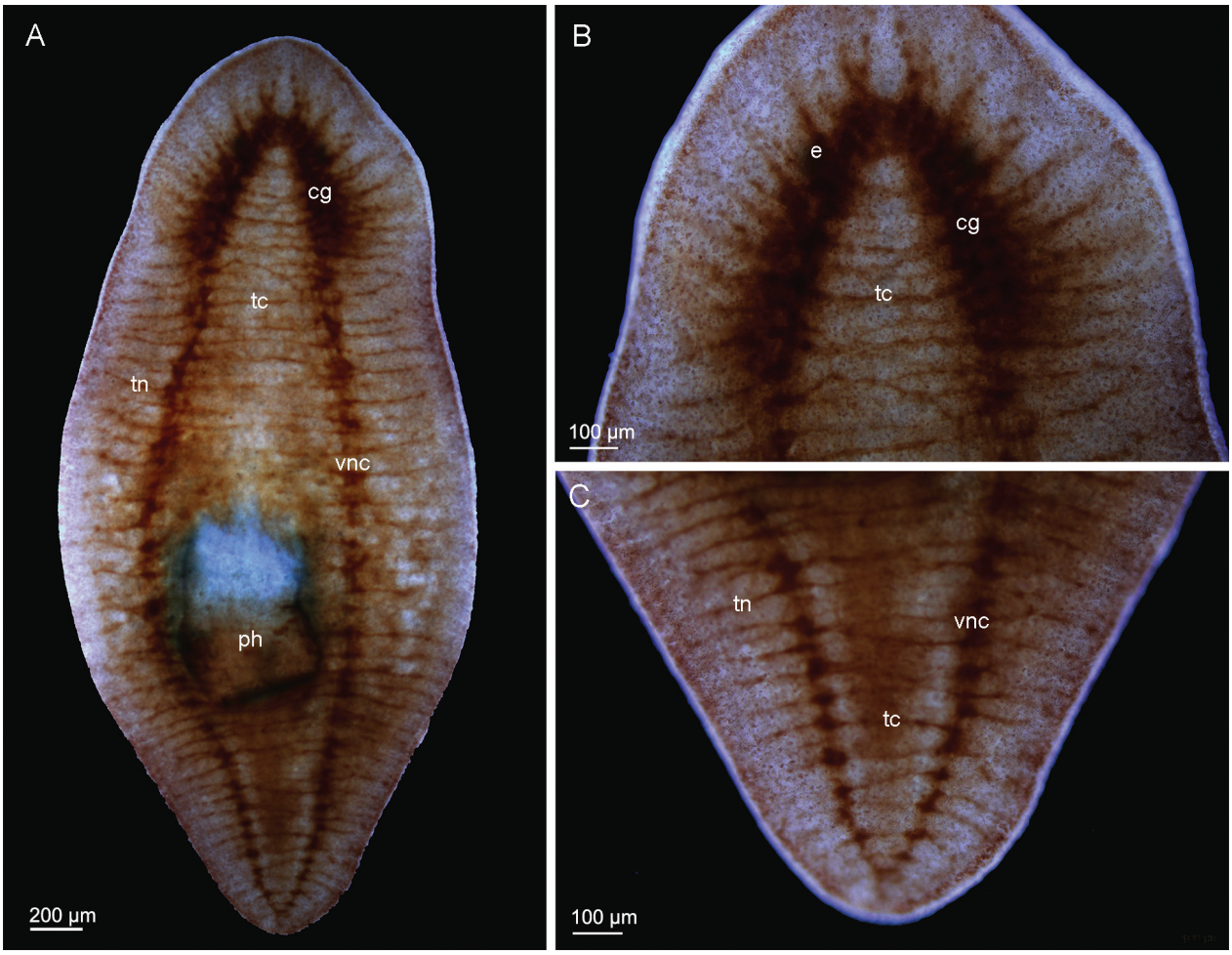

Figure 9. *Dugesia umbonata*, AChE nervous system structure, ventral view. **A.** entire animal; **B.** anterior end with cerebral ganglion; **C.** tail.

In none of the specimens examined, testes could be discerned. The penis consists of a plump, more or less barrel-shaped papilla and an elongated bulb, the latter consisting of intermingled longitudinal and circular muscle fibres (Figs 5B–D, 6B–D, 7B–D). The papilla is covered by a nucleated epithelium, which is underlain by 1–3 layers of circular muscles, followed by a layer of longitudinal muscle fibres.

The penis bulb houses an egg-shaped seminal vesicle, which is situated near the antero-ventral side of the penis bulb (Figs 5A, B, D, E, 6B, D, E, 7). The seminal vesicle is lined with a nucleated epithelium and surrounded by a layer of longitudinal muscle. The vasa deferentia open separately through the antero-dorsal wall of the seminal vesicle.

At its dorsal portion, the seminal vesicle gives rise to an extension that initially is rather broad, but then quickly narrows, while following a postero-ventral course to the small diaphragm, through which it communicates with the ejaculatory duct (Figs 5B–E, 6B–E, 7B–E). The seminal vesicle and its extension are lined with a cuboidal, nucleated epithelium, which is underlain by 2–4 layers of circular muscle fibres. The small conical diaphragm is covered by an infranucleated epithelium that is underlain by 1–2 subepithelial layers of circular muscle. The diaphragm receives the abundant secretion of erythrophil penis glands, which discharge their secretion also into the most proximal, anterior portion of the ejaculatory duct (Figs 5B–E, 6B–E, 7).

From the ventrally located diaphragm, the ejaculatory duct starts a postero-dorsally orientated course through the penis papilla, after a while exhibiting a dorsally directed knee-shaped bend, whereafter it opens subterminally through the dorsal side of the penis papilla, thus giving rise to an asymmetrical penis papilla (Figs 5B–E, 6B–E, 7B–E).

The male atrium is lined by an epithelium consisting of nucleated, cylindrical cells and it is surrounded by a subepithelial layer of circular muscle, followed by 2–3 layers of longitudinal muscle. The male atrium communicates with the common atrium via a pronounced constriction (Figs 5B, D, E, 6B–E, 7B–E). The common atrium is lined with a nucleated epithelium and is surrounded by a subepithelial layer of circular muscle, followed by a layer of longitudinal muscle. Abundant, erythrophilic cement glands discharge their secretion into the gonopore, gonoduct and the very ventral portion of the common atrium (Figs 5B, D, E, 6B–E, 7B–E). The gonopore is located at 1/3–1/4 ($n = 5$) of the body length, as determined from the posterior body margin (Fig. 4C).

Histochemical structure of the nervous system. After histochemical reaction with AChE, the major nervous system appears as a copper-red, ladder-like structure, comprising a brain, two ventral nerve cords and accompanying lateral branches and transverse commissures (Fig. 9). The brain is composed of the thickened anterior portions of the ventral nerve cords, thus forming the cerebral ganglia, which together form an inverted V-shaped or U-shaped brain, as the ganglia are connected by a commissure at their anterior ends (Fig. 9A, B). In addition, the ganglia communicate with each other by 6–7 thin, transverse commissures (n = 4; Fig. 9A, B). Each ganglion gives off 9–11 nerve branches (n = 4; Fig. 9A, B). The eyes lie at the lateral border of the cerebral ganglia (Fig. 9A, B). The two ventral nerve cords extend backwards from the posterior end of the cerebral ganglia and communicate at the tail end, giving off 43–47 lateral nerve branches on either side of the body (Fig. 9A, C), while there are 38–42 transverse commissures between the ventral nerve cords, which are especially numerous in the tail region (Fig. 9A, C). The lateral nerve branches communicate with the marginal or lateral nerve cords, which are only weakly developed (Fig. 9).

Discussion

The substitution saturation tests of the COI datasets (nos. 7 to 12 in Suppl. material 3: Table S3) revealed that gaps and ambiguous codes significantly influenced the accuracy of the tests. The results reveal that the COI dataset is actually substitutionally saturated (Iss > Iss.c; no. 7 in Suppl. material 3: Table S3) and, therefore, not suitable for phylogenetic reconstruction. The main reason for this resides in the presence of two rather short sequences, which will cause a great number of gaps during alignment. Inclusion of only the fully-resolved sites of the COI dataset (nos. 8, 10 and 12 in Suppl. material 3: Table S3) reduces the analysis to only a few sites and, thus, cannot represent the true level of substitution saturation. Hence, the real saturation level in the COI dataset is most likely closer to the results obtained with the aCOI dataset (nos. 13 and 14 in Suppl. material 3: Table S3) than that it reflects its current results (no. 7 in Suppl. material 3: Table S3), because numerous gaps have a greater influence during determination of the saturation than two missing sequences (*D. batuensis* and *D. deharvengi*). This implies that the COI dataset is more likely to experience little or no substitution saturation and, thus, would be reliable and valid and, in principle, suitable for phylogenetic analysis. Although the third codon position showed substitution saturation to a greater or lesser extent (nos. 17 and 18 in Suppl. material 3: Table S3), its inclusion, nevertheless, is to be preferred as, without it, the phylogenetic trees exhibit rather low resolution.

In the phylogenetic trees generated during the present study, *D. umbonata* occupies a single branch that shares a sister-group relationship either with *D. japonica* (in trees based on the 18S rDNA, 28S rDNA, COI and concatenated datasets; Fig. 1 and Suppl. material 4: Figs S1–S5) or with a clade formed by a group of species from the Australasian and Oriental regions (in the case of ITS-1; Suppl. material 4: Fig. S6). The long branch of *D. umbonata* in all phylogenetic trees signals its high divergence from other species and supports its separate specific status.

In the phylogenetic trees obtained from the separate 18S rDNA, 28S rDNA and COI datasets or from the concatenated dataset, the sister-group relationship between *D. umbonata* and *D. japonica* is robust, strongly suggesting that these two species belong to the same monophyletic group and are each other's closest relative (Fig. 1 and Suppl. material 4: Figs S1–S5).

It is unusual that five phylogenetic trees (based on 18S rDNA, 28S rDNA, COI, ITS-1 and the concatenated dataset; Fig. 1 and Suppl. material 4: Figs S1–S6) show rather different topologies. However, the trees resulting from the concatenated dataset (Fig. 1 and Suppl. material 4: Fig. S1) should be the most reliable ones, as these are based on all four genes, while a partition analysis was also applied. One could argue that the low support values are due to incongruence amongst the various molecular markers and that a concatenated dataset could be analysed with exclusion of COI. When this would result in higher support values, it would underscore removal of COI from the concatenated dataset. In point of fact, we did perform a phylogenetic analysis on such a restricted concatenated dataset which, surprisingly, had precisely the opposite effect, i.e. lowering the support values. Therefore, we kept COI in our concatenated dataset.

With respect to the trees independently generated from each of the four sequences, it should be noted that the reliabilities of 18S rDNA and 28SrDNA are lower than those of ITS-1 and COI, due to the limited number of 18S and 28S rDNA sequences involved in the analysis and the fact that the last-mentioned sequences are more conservative during evolution than ITS-1 and COI, implying that the latter provide more molecular signals for our level of analysis. That is also the reason why the phylogenetic trees based on COI and ITS-1 have topologies similar to those based on the concatenated dataset (Fig. 1 and Suppl. material 4: Figs S1–S3, S6). In the 18S rDNA tree, the clade comprising *D. umbonata* and *D. japonica* clusters with Afrotropical and Cameroon species (Suppl. material 4: Fig. S4), while it clusters with species from the western Palearctic region in the 28S rDNA tree (Suppl. material 4: Fig. S5). However, due to the low reliability of these trees (see above), we believe that *D. umbonata* and *D. japonica* actually belong to the Australasian and Oriental species group, as shown in the phylogenetic trees based on COI, ITS-1 and the concatenated dataset.

Although the major purpose of our phylogenetic analysis was to determine the phylogenetic position and taxonomic status of the new species *D. umbonata*, inclusion of four gene sequences of no less than 39 species of *Dugesia* in our BI and ML analyses makes it worthwhile to compare the topology of our tree with those generated

in several other, recent studies. Evidently, the different molecular markers used in the different studies, including ours, complicate proper evaluation and, therefore, we refrain from drawing any conclusions on the evolutionary relationships between the species.

In the tree of Harrath et al. (2019: fig. 2), the species *D. bijuga* Harrath & Sluys, 2019 and *D. pustulata* Harrath & Sluys, 2019 from Cameroon cluster together and are sister to a group constituted by Asian, Australian and European species. It is noteworthy that, in our phylogenetic trees based on COI, *D. bijuga* clusters with an Oriental species, viz. *D. batuensis*, albeit with rather low support (0.60 pp; 33% bs; Suppl. material 4: Figs S2, S3). However, in our other trees, based on ribosomal genes and the concatenated dataset, these two Cameroon species share the same affinities as revealed by Harrath et al. (2019), in that they cluster with Australasian, Oriental and Western Palearctic species.

Although we included in our analyses these two species of *Dugesia* from Cameroon that were recently described by Harrath et al. (2019), the topology of our tree, based on the concatenated dataset, is more similar to the one of Stocchino et al. (2017), which was based on ITS-1 and COI, than to the tree published by Harrath et al. (2019), based on 18S rDNA and COI. With respect to the biogeographic groupings identified in these studies, the five biogeographic groups indicated in our trees, based on the concatenated dataset, are basically similar to those in Harrath et al. (2019) and Stocchino et al. (2017). However, it should be noted that, although in the present study we included more genetic markers and a larger number of species, as compared with the studies of Stocchino et al. (2017) and Harrath et al. (2019), the number of *Dugesia* species for which molecular data are available (~40) is still rather small. Therefore, robust hypotheses on the historical biogeography of the genus *Dugesia* and the testing of previously-formulated ones (for an overview, see Harrath et al. 2019) may only be well possible when more molecular data have become available, notably from more and also better resolved markers.

Frequently, species of *Dugesia* are characterised only by a unique, diagnostic *combination* of features, while each of these characters separately occurs in many congeners. Much more rarely, a species exhibits an unambiguous apomorphic character or character state through which it can easily and quickly be diagnosed. Fortunately, *Dugesia umbonata* is an example of the last-mentioned situation, as it features a peculiar muscularised hump on the postero-dorsal portion of its bursal canal, a structure thus far unknown from any species of *Dugesia*. In addition, *D. umbonata* exhibits the unique condition in which its ejaculatory duct opens subterminally through the dorsal side of the penis papilla. Although other species of *Dugesia* may also show subterminal openings (see Stocchino et al. 2017 and references therein), these are located on the ventral side of the penis papilla, with the only exception of *D. hepta* Pala et al., 1981, in which the opening is located laterally (Stocchino et al. 2005). Therefore, the condition in *D. umbonata* (subterminal and dorsal opening of ejaculatory duct) represents an apomorphy.

Other noteworthy features of *D. umbonata* are the asymmetrical openings of the oviducts and the presence of a duct between the seminal vesicle and the diaphragm, representing character states 11-1 and 5-1, respectively, in the phylogenetic analysis of Sluys et al. (1998). Amongst the already-described species of *Dugesia*, the combination of these two character-states occurs only in *D. notogaea* Sluys & Kawakatsu, 1998 and *D. sudanica* Dahm, 1971 (Dahm 1971; Sluys et al. 1998). However, both species are different from *D. umbonata* as, for example, neither of them exhibits the muscular hump on the bursal canal.

In view of the fact that, in most of our molecular analyses and particularly in the tree based on the concatenated dataset (Fig. 1), *D. umbonata* was the sister-species of *D. japonica* and that the latter occurs also in China (Kawakatsu et al. 1995), it is opportune to discuss the similarities and differences between these two species in some more detail. In particular, it is noteworthy that specimens of *D. japonica* have been described in which the vaginal region of the bursal canal is surrounded by a "…very wide halo-like structure…[consisting of] …mesenchymal tissue traversed by several coarse rows of longitudinal muscles and less-developed radial ones" (Kawakatsu et al. 1976: p. 85). This is reminiscent of the muscularised hump in *D. umbonata* (cf. Kawakatsu et al. 1976: fig. 3), but frequently, this thick coat of muscles in *D. japonica* gradually expands and thereafter also gradually decreases in diameter towards the copulatory bursa (cf. Kawakatsu et al. 1979: fig. 3), while it is developed also ventrally to the bursal canal (cf. Kawakatsu et al. 1976: figs 5, 8; Kawakatsu et al. 1980: fig. 2A). This contrasts with the situation in *D. umbonata*, in which the muscular hump is confined to the dorsal side of the bursal canal and also has a much more clearly-defined shape and proportions. Evidently, other differences also preclude assignment of our newly-collected specimens to *D. japonica*. For example, in *D. japonica*, the oviducts open symmetrically into the bursal canal, whereas in *D. umbonata*, the oviducal openings are highly asymmetrical. Another clear difference between both species concerns the location of the subterminal opening of the ejaculatory duct at the tip of the penis papilla. *Dugesia japonica* expresses the condition that is rather common amongst a group of *Dugesia* species distributed in the Palearctic, Afrotropical, Oriental, Sino-Japanese and Australian regions, i.e. a subterminal ventral opening (cf. Sluys et al. 1998), whereas *D. umbonata* exhibits the unique character state of a subterminal dorsal opening.

Hyperplasic ovaries are a common feature of sexualised planarians from originally fissiparous populations (cf. Stocchino et al. 2012 and references therein) and, thus, were expected to occur in the sexualised specimens of *D. umbonata*. Regularly, hyperplasic ovaries in such

ex-fissiparous specimens go together with under-developed testes or even with complete absence of testicular follicles (cf. Stocchino et al. 2012 and references therein). The latter condition is present also in *D. umbonata* as we were unable to discern testis follicles in any of the specimens examined, coinciding with the fact that, in our cultures, we never found cocoons.

The major nerve system of *D. umbonata*, as documented above, may be compared with three of its congeners for which the structure of the nerve system was described, viz. *Dugesia gonocephala* (Dugès, 1830), *D. japonica* and *D. sinensis* Chen & Wang, 2015. As studies on these three species and *D. umbonata* were done with different techniques (e.g. various immunocytochemical methods, acetylcholinesterase (AChE) histochemistry, traditional histology), some caution should be taken in comparing their results. However, as our focus is on the gross morphology of the nervous system, it is well possible to compare the neuroanatomical results of these studies with our results on *D. umbonata*.

The shape of the planarian brain probably is correlated with the shape of the head, with triangular heads tending to have brains composed of thickened anterior portions of the ventral nerve cords that form two lobes or cerebral ganglia and truncate heads having more rounded, bilobed cerebral ganglia (Hyman 1951; Reuter et al. 1995), while in land planarians, the ventral nerve plate extends to the anterior tip and may expand into the lunate head of species of *Bipalium* Stimpson, 1858 (Hyman 1951; Rieger et al. 1991). In that respect, the shape of the brain is similar in all four species of *Dugesia* in that it consists of the thickened anterior portions of the ventral nerve cords, which are connected by a major commissure at their anterior ends, while the eyes are located at a short distance posterior to this commissure and at the lateral margins of the thickened lobes (cf. Ude 1908; Umesono et al. 2011; Chen et al. 2015). In all four species, the lateral nerves communicate with the marginal nerves, which are much less condensed than the ventral nerve cords or the transverse and lateral branches and basically consist of a peripheral submuscular nerve plexus (cf. Chen et al. 2015: fig. 16). In *D. gonocephala*, *D. japonica* and *D. sinensis*, the major ventral nerve cords are not confluent in the very tail end of the body (Ude 1908; Nishimura et al. 2010; Chen et al. 2015), whereas in *D. umbonata* the cords pass into each other (Fig. 8A, C).

In *D. gonocephala*, Ude (1908) counted 47 transverse commissures and 51–64 lateral branches, while in *D. japonica* (46–54 lateral branches; 37–40 transverse commissures; Nishimura et al. 2010) and *D. umbonata* (43–47 lateral branches; 38–42 transverse commissures; this study), the numbers are somewhat lower. For *D. sinensis*, the numbers are considerably lower, viz. 21–24 transverse commissures and 28 lateral branches (from Chen et al. 2015: fig. 16).

For the number of transverse commissures between the two ganglia and the number of lateral branches arising from the brain, the following data have been reported, respectively: *D. gonocephala*: 8, 8 (Ude 1908); *D. sinensis*: 7–8, 9–10 (from Chen et al. 2015: fig. 16; Chen et al. 2015, respectively); *D. japonica*: 6, ± 9 (Nishimura et al. 2010; Umesono et al. 2011). These figures are in the same order of magnitude as the branches in *D. umbonata*, viz. 6–7 transverse commissures between the ganglia and 9–11 lateral branches arising from each cerebral ganglion.

Acknowledgements

This study was supported by Special Funds for the Cultivation of Guangdong College Students' Scientific and Technological Innovation ("Climbing Program" Special Funds; grant no. pdjh2020b0509); a Shenzhen Science and Technology Application Demonstration project (grant no. KJYY20180201180253571); a China Undergraduate Training Program for Innovation and Entrepreneurship (grant no. 201910590033) and the Shenzhen University Innovation Development Fund (grant no. 2019272). We are grateful to Xiao-Zhou Hu for collecting the samples, Zhong-Yin Sun for culturing the animals in lab and Yi-Tao Lin for assistance with the PCR. We thank Dr. Fang-Luan Gao (Fujian Agriculture and Forestry University, China), Dr. Yu Zhang (Shenzhen University, China) and Si-Yu Zhang for their kind help and useful suggestions on molecular phylogeny. Yuki Oya from Hokkaido University (Japan) is also thanked for making available literature on Japanese *Dugesia* species. We also thank Jun-Yu Li, Jia-Jia Chen, Ying Yang and Ming-Qi Wu for their kind support in the laboratory. Wei-Xuan Li would like to express his gratitude to all members, as well as supervisors, in Wang's lab for their companionship and support during this study and, more importantly, during his four-year academic journey at Shenzhen University. We thank reviewer Dr. M. Álvarez-Presas and also an anonymous reviewer for their constructive comments and encouragement.

References

Chen G-W, Lü J-Q, Ma J-Y, Liu D-Z (2001) Report on freshwater planarians from China. Acta Zoologica Sinica 47: 9–12. [In Chinese]

Chen Y-H, Chen X-M, Wu C-C, Wang A-T (2015) A new species of the genus *Dugesia* (Tricladida: Dugesiidae) from China. Zoological Systematics 40: 237–249. https://doi.org/10.11865/zs.20150301

Dahm AG (1971) *Dugesia sudanica* sp.n. from Africa (Turbellaria, Tricladida, Paludicola). Zoologica Scripta 1: 37–41. https://doi.org/10.1111/j.1463-6409.1971.tb00711.x

Harrath AH, Sluys R, Mansour L, Folefack GL, Aldahmash W, Alwasel S, Solà E, Riutort M (2019) Molecular and morphological identification of two new African species of *Dugesia* (Platyhelminthes, Tricladida, Dugesiidae) from Cameroon. Journal of Natural History 53: 253–271. https://doi.org/10.1080/00222933.2019.1577508

Hyman LH (1951) The Invertebrates: Platyhelminthes and Rhynchocoela. McGraw Hill, New York, 550 pp.

Kawakatsu M, Oki I, Tamura S (1995) Taxonomy and geographical distribution of *Dugesia japonica* and *D. ryukyuensis* in the Far East. Hydrobiologia 305: 55–61. https://doi.org/10.1007/BF00036363

Kawakatsu M, Oki I, Tamura S, Sugino H (1976) Studies on the morphology, karyology and taxonomy of the Japanese freshwater planarian *Dugesia japonica* Ichikawa et Kawakatsu, with a description of a new subspecies, *Dugesia japonica ryukyuensis* subspec. nov. Bulletin of the Fuji Women's College no. 14, ser. II: 81–126.

Kawakatsu M, Oki I, Tamura S, Yamayoshi T, Takahashi N (1980) Morphological, karyological and taxonomic studies of *Dugesia japonica* Ichikawa et Kawakatsu from the Tsushima Islands. Proceedings of the Japanese Society of Systematic Zoology 19: 1–10. [2 pls.] https://doi.org/10.19004/pjssz.19.0_1

Kawakatsu M, Oki I, Tamura S, Yamayoshi T, Lue KY, Hagiya M (1979) Additional report on freshwater planarians from Taiwan. Bulletin of the Fuji Women's College no. 17, ser. II: 59–91.

Kozlov AM, Darriba D, Flouri M, Morel B, Stamatakis A (2019) RAxML-NG: a fast, scalable and user-friendly tool for maximum likelihood phylogenetic inference. Bioinformatics 35(21): 4453–4455. https://doi.org/10.1093/bioinformatics/btz305

Li W-X, Sluys R, Vila-Farré M, Chen J-J, Yang Y, Li S-F, Wang A-T (2019) A new continent in the geographic distribution of the genus *Oregoniplana* (Platyhelminthes: Tricladida: Maricola), its rediscovery in South Africa and its molecular phylogenetic position. Zoological Journal of the Linnean Society 187: 82–99. https://doi.org/10.1093/zoolinnean/zlz013

Nishimura K, Kitamura Y, Taniguchi T, Agata K (2010) Analysis of motor function modulated by cholinergic neurons in planarian *Dugesia japonica*. Neuroscience 168: 18–30. https://doi.org/10.1016/j.neuroscience.2010.03.038

Nylander JAA (2004) MrModeltest v2. Program distributed by the author. Evolutionary Biology Centre, Uppsala University.

Rambaut A, Drummond AJ, Xie D, Baele G, Suchard MA (2018) Posterior summarisation in Bayesian phylogenetics using Tracer 1.7. Systematic Biology 67: 901–904. https://doi.org/10.1093/sysbio/syy032

Ranwez V, Harispe S, Delsuc F, Douzery EJP (2011) MACSE: Multiple Alignment of Coding SEquences accounting for frameshifts and stop codons. PLoS ONE 6(9): e22594. https://doi.org/10.1371/journal.pone.0022594

Reuter M, Gustafsson MKS, Sheiman IM, Terenina N, Halton DW, Maule AG, Shaw C (1995) The nervous system of Tricladida. II. Neuroanatomy of *Dugesia tigrina* (Paludicola, Dugesiidae): an immunocytochemical study. Invertebrate Neuroscience 1: 133–143. https://doi.org/10.1007/BF02331911

Rieger RM, Tyler S, Smith III JPS, Rieger G (1991) Platyhelminthes: Turbellaria. In: Harrison FW, Bogitsh BJ (Eds) Microscopic Anatomy of the Invertebrates, 3. Wiley-Liss, New York, 7–140.

Ronquist F, Teslenko M, van der Mark P, Ayres DL, Darling A, Höhna S, Larget B, Liu L, Suchard MA, Huelsenbeck JP (2012) MrBayes 3.2: efficient Bayesian phylogenetic inference and model choice across a large model space. Systematic Biology 61: 539–542. https://doi.org/10.1093/sysbio/sys029

Sluys R, Riutort M (2018) Planarian diversity and phylogeny. In: Rink JC (Ed.) Planarian Regeneration: Methods and Protocols. Methods in Molecular Biology (Vol. 1774). Humana Press, Springer Science+Business Media, New York, 1–56. https://doi.org/10.1007/978-1-4939-7802-1_1

Sluys R, Kawakatsu M, Winsor L (1998) The genus *Dugesia* in Australia, with its phylogenetic analysis and historical biogeography (Platyhelminthes, Tricladida, Dugesiidae). Zoologica Scripta 27: 273–289. https://doi.org/10.1111/j.1463-6409.1998.tb00461.x

Stocchino GA, Sluys R, Manconi R (2012) A new species of *Dugesia* (Platyhelminthes, Tricladida, Dugesiidae) from the Afromontane forest in South Africa, with an overview of freshwater planarians from the African continent. Zootaxa 3551: 43–58. https://doi.org/10.11646/zootaxa.3551.1.3

Stocchino GA, Corso G, Manconi R, Casu S, Pala M (2005) Endemic freshwater planarians of Sardinia: Redescription of *Dugesia hepta* (Platyhelminthes, Tricladida) with a comparison of the Mediterranean species of the genus. Journal of Natural History 39: 1947–1960. https://doi.org/10.1080/00222930500060025

Stocchino GA, Sluys R, Riutort M, Solà E, Manconi R (2017) Freshwater planarian diversity (Platyhelminthes: Tricladida: Dugesiidae) in Madagascar: new species, cryptic species, with a redefinition of character states. Zoological Journal of the Linnean Society 181: 727–756. https://doi.org/10.1093/zoolinnean/zlx017

Talavera G, Castresana J (2007) Improvement of phylogenies after removing divergent and ambiguously aligned blocks from protein sequence alignments. Systematic Biology 56: 564–577. https://doi.org/10.1080/10635150701472164

Tamura K, Stecher G, Peterson D, Filipski A, Kumar S (2013) MEGA6: molecular evolutionary genetics analysis version 6.0. Molecular Biology and Evolution 30: 2725–2729. https://doi.org/10.1093/molbev/mst197

Ude J (1908) Beiträge zur Anatomie und Histologie der Süßwassertricladen. Zeitschrift für wissenschaftliche Zoologie 89: 308–370. [2 pls.]

Umesono Y, Tasaki J, Nishimura K, Inoue T, Agata K (2011) Regeneration in an evolutionarily primitive brain – The planarian *Dugesia japonica* model. European Journal of Neuroscience 34: 863–869. https://doi.org/10.1111/j.1460-9568.2011.07819.x

Xia X (2017) DAMBE6: New tools for microbial genomics, phylogenetics and molecular evolution. Journal of Heredity 108: 431–437. https://doi.org/10.1093/jhered/esx033

Xia X, Lemey P (2009) Assessing substitution saturation with DAMBE. In: Lemey P, Salemi M, Vandamme A (Eds) The Phylogenetic Handbook: A Practical Approach to Phylogenetic Analysis and Hypothesis Testing. University Press, Cambridge, 615–630. https://doi.org/10.1017/CBO9780511819049.022

Xia X, Zheng X, Salemi M, Chen L, Wang Y (2003) An index of substitution saturation and its application. Molecular Phylogenetics and Evolution 26: 1–7. https://doi.org/10.1016/S1055-7903(02)00326-3

Yang Y, Li J-Y, Sluys R, Li W-X, Li S-F, Wang A-T (2020) Unique mating behavior, and reproductive biology of a simultaneous hermaphroditic marine flatworm (Platyhelminthes, Tricladida, Maricola). Invertebrate Biology 139: e12282. https://doi.org/10.1111/ivb.12282

Supplementary material 1

Table S1. Primer sequences used for PCR amplification

Authors: Xiao-Yu Song, Wei-Xuan Li, Ronald Sluys, Shu-Xin Huang, Shuang-Fei Li, An-Tai Wang
Data type: molecular data

Link: https://doi.org/10.3897/zse.96.52484.suppl1

Supplementary material 2

Table S2. Preparation of solutions and reagents used in AChE histochemical study

Authors: Xiao-Yu Song, Wei-Xuan Li, Ronald Sluys, Shu-Xin Huang, Shuang-Fei Li, An-Tai Wang
Data type: methods

Link: https://doi.org/10.3897/zse.96.52484.suppl2

Supplementary material 3

Table S3. The index of substitution saturation (Iss) values of 5 datasets

Authors: Xiao-Yu Song, Wei-Xuan Li, Ronald Sluys, Shu-Xin Huang, Shuang-Fei Li, An-Tai Wang
Data type: molecular data

Link: https://doi.org/10.3897/zse.96.52484.suppl3

Supplementary material 4

Figures S1–S6

Authors: Xiao-Yu Song, Wei-Xuan Li, Ronald Sluys, Shu-Xin Huang, Shuang-Fei Li, An-Tai Wang
Data type: phylogenetic tree
Explanation note: **Fig. S1.** Bayesian inference phylogenetic tree topology inferred from the concatenated dataset. **Fig. S2.** Bayesian inference phylogenetic tree based on COI dataset. **Fig. S3.** Maximum likelihood phylogenetic tree based on COI dataset. **Fig. S4.** Maximum likelihood phylogenetic tree based on COI dataset. **Fig. S5.** Maximum likelihood phylogenetic tree topology based on 28S rDNA dataset. **Fig. S6.** Maximum likelihood phylogenetic tree based on ITS-1 dataset.

Link: https://doi.org/10.3897/zse.96.52484.suppl4